Journal of Microscopy

Journal of Microscopy, Vol. 260, Issue 1 2015, pp. 47–61 doi: 10.1111/jmi.12265
Received 18 December 2014; accepted 13 April 2015

Optimizing use of the structural chemical analyser (variable pressure FESEM-EDX raman spectroscopy) on micro-size complex historical paintings characterization

I. GUERRA* & C. CARDELL†
*Scientific Instrumentation Centre, Avda. Campus Fuentenueva, University of Granada, 18071 Granada, Spain
†Department of Mineralogy and Petrology, Faculty of Science, University of Granada, Campus Fuentenueva s/n, 18071 Granada, Spain

Key words. Historical paintings, hyphenated VP-FESEM-EDX Raman spectroscopy, optimization procedure, Structural Chemical Analyser.

Summary

The novel Structural Chemical Analyser (hyphenated Raman spectroscopy and scanning electron microscopy equipped with an X-ray detector) is gaining popularity since it allows 3-D morphological studies and elemental, molecular, structural and electronic analyses of a single complex micro-sized sample without transfer between instruments. However, its full potential remains unexploited in painting heritage where simultaneous identification of inorganic and organic materials in paintings is critically yet unresolved. Despite benefits and drawbacks shown in literature, new challenges have to be faced analysing multifaceted paint specimens. SEM–Structural Chemical Analyser systems differ since they are fabricated *ad hoc* by request. As configuration influences the procedure to optimize analyses, likewise analytical protocols have to be designed *ad hoc*. This paper deals with the optimization of the analytical procedure of a Variable Pressure Field Emission scanning electron microscopy equipped with an X-ray detector Raman spectroscopy system to analyse historical paint samples. We address essential parameters, technical challenges and limitations raised from analysing paint stratigraphies, archaeological samples and loose pigments. We show that accurate data interpretation requires comprehensive knowledge of factors affecting Raman spectra. We tackled: (i) the in-FESEM–Raman spectroscopy analytical sequence, (ii) correlations between FESEM and Structural Chemical Analyser/laser analytical position, (iii) Raman signal intensity under different VP-FESEM vacuum modes, (iv) carbon deposition on samples under FESEM low-vacuum mode, (v) crystal nature and morphology, (vi) depth of focus and (vii) surface-enhanced Raman scattering effect. We recommend careful planning of analysis strategies prior to research which, although time consuming, guarantees reliable results. The ultimate goal of this paper is to help to guide future users of a FESEM-Structural Chemical Analyser system in order to increase applications.

Correspondence to: Carolina Cardell, Department of Mineralogy and Petrology, Faculty of Science, University of Granada, Campus Fuentenueva s/n, 18071 Granada, Spain. Tel: (+34)958242725; fax: (+34)958243368); e-mail: cardell@ugr.es

Introduction

The Structural Chemical Analyser (SCA) system is a unique and potent combination of two full-grown technologies designed to obtain, in a single hybridized instrument, morphological and elemental information from scanning electron microscopy-energy-dispersive X-ray spectroscopy (SEM-EDX) with molecular, structural and electronic data from Raman spectroscopy (RS). SCA enables identification of organic and inorganic compounds on the same sample without restrictions of the sequential use of SEM-EDX and RS (Jarvis *et al.*, 2004; Toepfer & Shearer, 2006; Otieno-Alego, 2009; Worobiec *et al.*, 2010; Goienaga *et al.*, 2013). This novel technique is commercialized by *Renishaw* (Renishaw plc., Gloucestershire, UK) since 2003 (http://www.renishaw.com). Although SEMs-EDX information includes morphology and mean atomic number from secondary (SE) and backscattered (BSE) electrons, respectively, and elemental composition from EDX analysis, SEMs are not suited for structural analysis which limits their application towards organic chemistry and life sciences. By contrast, RS analyses vibrational, rotational and other low-frequency modes in a system, providing molecular, structural and physical information, so that both inorganic and organic compounds can be identified.

The advantage of using in-SEM Raman analysis instead of RS equipped with an optical microscope (micro-Raman spectroscopy, MRS hereafter) lies in the fact that SEMs provide accuracy in visualizing features on studied samples. SEMs overcome limitations of MRS (even more using a field emission scanning electron microscopes [FESEM]) with regard to spatial resolution (3–4 orders of magnitude better than optical

microscopy), depth of field and contrast (from surface topography and mean atomic number), such that the capability to identify and analyse a region of interest (ROI hereafter) is much more accurate and easier than using MRS. On the contrary, Raman bands are more intense in MRS.

At present, SEM–SCA systems are limited to relatively few research centres and laboratories, many not accessible to the research community since they are housed in police forensics departments or private Institutions. Likewise and consequentially, literature on SCA application is sparse. In-SEM Raman analyses cover diverse fields, but few articles have been published yet. Pioneering works began in 1986 by Truchet & Delhaye (1988) proposing a hyphenated system to perform Raman analyses within an electronic microscope. In 2003, *Renishaw* launched the SCA technique and presented the advantages of its use in diverse fields (Williams *et al.*, 2003; Brooker *et al.*, 2003; Prusnick *et al.*, 2004; Brooker *et al.*, 2004; Kawauchi *et al.*, 2004). Since 2004, in-SEM Raman analyses have been used to identify bacteria (Jarvis *et al.*, 2004), mineral particles and aerosols (Stefaniak *et al.*, 2006; Worobiec *et al.*, 2010; Worobiec *et al.*, 2011), slag (Gómez-Nubla *et al.*, 2013), uranium compounds (Pointurier & Marie, 2013; Stefaniak *et al.*, 2014), metal-rich particles (Goienaga *et al.*, 2013), for criminalistics purposes (Otieno-Alego, 2009) and to solve biological problems (Van Apeldoorn *et al.*, 2005; Hazekamp *et al.*, 2011; López-Sánchez *et al.*, 2011). In the field of heritage science, SEM–SCA has been applied to typify clayey earth pigments (Ospitali *et al.*, 2008), archaeological pottery (Bersani *et al.*, 2010) and ancient bronzes (Ospitali *et al.*, 2012).

Certainly, in-SEM Raman analyses open new insight to characterize micro- and nanoscaled complex composite compounds. However, concurrently, new practical challenges have to be faced since analyses are less obvious than expected. Indeed *Renishaw* provides SEM recommendations to work with SCA since the procedure to obtain good Raman spectra is particularly challenging. Few papers address difficulties found characterizing samples with SCA, suggesting that the analytical process needs supplemental optimization (Stefaniak *et al.*, 2006; Worobiec *et al.*, 2010; Cardell *et al.*, 2013; Wille *et al.*, 2014), as we show here.

The SCA interface can be fitted to different SEM models. Thus, RS is compatible with low- and high-vacuum conditions (LVC and HVC hereafter), although RS under environmental scanning electron microscope mode is not possible. RS can also be fitted to field emission (high resolution) scanning electron microscopes (FESEM). More recently, cryo SEM has been coupled to MRS (Hazekamp *et al.*, 2011; López-Sánchez *et al.*, 2011). Indeed, each SEM–SCA system is fabricated *ad hoc* by request. The Scientific Instrumentation Center (CIC) of the University of Granada (Spain) hosts a variable-pressure FESEM-EDX–SCA system since 2012 and launched the technique to the research community in 2013. Although the literature offers suggestions to overcome problems when analysing micro-sized mineral particles, we faced new difficulties using our FESEM-EDX–SCA to characterize hybrid mineral/organic nanocomposite paint samples.

Until now samples with relatively simple composition, i.e. with purely organic or purely inorganic construction (e.g. bacteria, metals, or mineral particles) have been analysed (Jarvis *et al.*, 2004; Bersani *et al.*, 2010; Worobiec *et al.*, 2011). Biocrystals (pearls) have been studied as well, although only the inorganic fraction was analysed (Wille *et al.*, 2014). Likewise, studies conducted on pigments and wall paintings ($CaCO_3$ is the binding media) showed only results of the mineral phases (Ospitali *et al.*, 2008; Wille *et al.*, 2014). In the CIC, SCA is demanded by experts in heritage science to examine artworks of complex composition with artistic and historic value. Specifically identification of concurrent pigments and binders in microlayers of paint stratigraphies (prepared as thin sections) is one of the most required but also challenging tasks. This work presents the optimization of the variable pressure FESEM-EDX–SCA analytical procedure to acquire the best analyses and results of historical painting materials. To this end, we address key parameters, technical challenges and limitations of the SCA and discuss problems that are both challenging and clearly time consuming. In a follow-up study, we will focus on the characterization of mock-ups and chip and resin-embedded paint samples applying our optimized analytical procedure.

Experimental section

Instrumentation

Our SEM–SCA comprises a FESEM which is a high resolution variable pressure SEM-EDX, a Raman spectrometer and the SEM–Raman interface (SCA interface). The FESEM is a *Zeiss Supra 40Vp* equipped with SE (InLens) and BSE detectors that provides morphological and chemical images, respectively, and a microanalysis system (*Aztec 2.2*) to deliver elemental analyses by EDX. The EDX detector is a 50 mm^2 silicon drift detector XMAX enabling detection of elements with $Z \geq 4$ (Be) and high count rates. The Raman spectrometer is a *Renishaw In Via* fitted with a Nd:YAG 532nm laser and a near infrared diode 785 nm laser, with maximum powers of 500 mW and 100 mW, respectively. It is coupled to a Peltier-cooled CCD detector and single-grating monochromators (1200 and 1800 lines mm^{-1}). It also houses a video system and white light illuminator used to locate a ROI. The FESEM and RS are coupled via the SCA interface, a retractable arm that is inserted into the FESEM between the final lenses and the FESEM stage. This device introduces laser light into the FESEM focused on the sample using a 50X objective; additionally it collects the Raman signal through the RS. Both laser light and the Raman signal are transmitted between the SCA and RS via optical fibre.

Raman analyses can be done simultaneously with SE imaging inside the FESEM. However, to acquire EDX and

BSE images the SCA arm must be retracted from the FESEM. Hypothetically the electron and the laser beams are confocal enabling sequencing of SEM, EDX and Raman results on the same ROI with micrometric precision without sample transfer. However, as we will see, the accuracy setting of the analytical position where the laser hits the sample is one of the main drawbacks of the SCA technique. Additionally, an analogue *Renishaw InVia* Reflex micro-Raman spectrometer equipped with a Peltier-cooled CCD detector coupled to a Leika confocal microscope was used to analyse individual pigments. The aim was to check if results acquired with MRS and FESEM–SCA were comparable in terms of Raman intensities.

Samples and measurements

We analysed loose pigments and historical paint stratigraphies prepared as polished thin sections, i.e. polychromes from the Alhambra monument (Granada, Spain) described elsewhere (Cardell *et al.*, 2009) and an archaeological sample from the hull of the *Bucentaur* ship. Samples were analysed with the FESEM–SCA using the 532 nm and 785 nm laser; previously, the Raman spectrometer was calibrated with the silicon 520.6 cm^{-1} Raman band. The type of laser and power, spectra accumulations, irradiation exposure time sand FESEM vacuum modes were different according to the studied sample and the parameter addressed (SCA set-up conditions are specified for each sample in the text). Likewise Raman spectra were recorded over different wavenumbers according to the sample, typically between 100–1600 cm^{-1} and 100–3200 cm^{-1}. Raman spectral data were acquired using *Renishaw* v.2.3 WiRE software. Laser spot size was *ca.* 2 μm. Laser power was controlled using neutral density filters to avoid degradation of samples. Baseline correction was not performed. Raman spectra interpretation was done with the open access RRUFF library (http://rruff.info/) and the *Renishaw* Minerals and Inorganic Materials Database R02-S/N H12345.

Single-point analyses were acquired on samples using VP-FESEM-EDX (20keV beam energy and 10 eV ch^{-1} resolution) to identify elemental composition of ROI. Samples were analysed under LVC (133Pa, the minimum vacuum level allowed in our FESEM). However, analyses at HVC (10^{-6} Torr) were also performed to check if the atmosphere of analysis influences Raman spectra. Samples were mounted on Al stubs with double-sided adhesive C tape. To check the SERS effect Al tapes were also used and samples were sputtered with gold nanoparticles (1–3 nm) using a *Polaron* SC7640 sputter coater. Samples were not carbon coated to obtain realistic Raman signals since carbon is Raman active.

Results and discussion

In-FESEM–RS analytical sequence

The logical sequence to work with an in-SEM Raman system is to collect images and chemical information with SEM via the following sequence: morphological SE images, elemental BSE images and EDX elemental analyses. This analytical sequence guides Raman molecular characterization of a ROI while ensuring that analyses are performed on the same area with SEM and the Raman laser. This recommended procedure is based on the fact that SEMs provide better resolution and morphological images than those acquired with MRS. Particularly, it is wise to follow this sequence in complex samples where goals are to characterize: (i) crystals/grains of few micrometres in size embedded in a matrix, such as pigments and binders mixed in multilayered paints (Irazola *et al.*, 2012; Wille *et al.*, 2014) or pigments present in glazes (Bersani *et al.*, 2010); (ii) individual particles (Stefaniak *et al.*, 2006; Worobiec *et al.*, 2010; Gómez-Nubla *et al.*, 2013) and (iii) compounds inserted in micrometric particles (Pointurier & Marie, 2013).

The analytical routine is rational considering that the spatial resolution and depth of field of MRS is much poorer than in SEM, even more using a FESEM. Although image spatial resolution in MRS is *ca.* 1–2 μm, it is *ca.* 3 nm for conventional SEMs and *ca.* 1 nm for FESEM. Unlike MRS, SEMs thus provide detailed morphological information (SE mode) of a ROI, facilitating the exploration of a target area. However, identification of the ROI has to be also realized with BSE chemical images followed by EDX elemental analyses since both restrain the searching of target areas within a complex sample. Finally, Raman analyses should be performed. The disadvantage of this procedure is long-term electron beam exposure, such that several nondesirable collateral effects arise which can compromise reliable Raman data; these include carbon deposition on samples, and damage induced by the vacuum and the electron. Therefore, depending on the aim of the investigation the analytical sequence can be changed, such that Raman spectra can be acquired first (Stefaniak *et al.*, 2014).

Correlation between FESEM and SCA/laser analytical position

The accurate correlation between the ROI studied under SEM and the analytical position of the Raman analysis is crucial to overcome limitations arising from using different excitation sources (electron and laser beams) and different focusing devices (electromagnetic lenses, optical lenses and parabolic mirrors), such that morphological, elemental and molecular information come from the same area. It is worth noting some essential factors to better assess this topic. The elemental and morphological study with SEMs shares the same excitation source, i.e. the electron beam. Thus the morphological image and the EDX analysed spot are perfectly correlated. In the case of RS coupled with an optical microscope (MRS), while the microscope uses white light to illuminate the ROI, the RS uses laser excitation to analyse it. However, both the RS and the optical microscope share optics and thus the white light and laser beam are mechanically aligned. On the other hand, the SEM–SCA uses an electron beam and a laser source which are focused by electromagnetic and optical systems, respectively.

Hence, we must guarantee that the electron beam and the laser beam are aligned to enable data acquisition on the very same ROI. To ensure beam alignment the SEM–SCA only has a CCD which delivers the optical image of the ROI.

To address this topic we considered the suggestions provided by *Renishaw* and the literature (Stefaniak *et al.*, 2006; Worobiec *et al.*, 2010). From reading the literature is not always evident that coincidence among SEM images, EDX analysis and Raman analysis is achieved. Relocation of a ROI with no micrometric precision is not a limitation when analysing homogeneous large areas were a misalignment of few micrometres is not essential (Goienaga *et al.*, 2013; Wille *et al.*, 2014) or analysing typically shaped crystals/particles which are easily identifiable using the white light image provided by the SCA Raman (Worobiec *et al.*, 2010, 2011). However, if complex compounds of few micrometres in size embedded in a matrix are analysed, additional caution has to be taken as the white light image provided by the SCA Raman is a poor image since it is collected by a parabolic mirror. Thus it is quite difficult to recognize the correspondence between optical and electronic features. This aspect is particularly challenging when particles are attached (such as our pigments with common $\varphi < 10$ μm) and embedded in layers of a paint stratigraphy. Since relocation of a ROI is based on typical particle contours, targeting agglomerate pigments mixed with organic binders inserted into a resin is quite challenging. This may explain why studies on these types of historical samples are lacking in the literature.

Our first approach to correlate a ROI between FESEM and RS was using the installation settings provided by *Renishaw* on a noncomplex archaeological sample taken from the hull of the *Bucentaur* ship. Its cross-section was prepared as a polished thin section using a polyester resin. This is a conductive sample made of fresh and degraded Cu layers which does not contain organic binders (which would cause Raman fluorescence). Although the *Renishaw* installation settings state that system design ensures reproducible positioning of the collection optics to submicrometres accuracy, surprisingly, we could identify a mismatch between the electronic and the laser beams because the laser beam impinged, not the Cu crystal marked with the crosshair in Figure 1, but rather the resin of the cross-section creating a hole.

A successful solution mentioned in literature to relocate aerosol particles is the use of Cu grids to create a type of coordinate system (Stefaniak *et al.*, 2006; Worobiec *et al.*, 2010). Hence to check beam alignment we used a Cu grid which offers an image with easily recognizable features. Perplexingly, we confirmed that there was a misalignment between the point impacted by the laser and the real point hit by the laser shown in the CCD image. We confirmed that despite relocating the sample position to the chosen site observed in the CCD image by moving the FESEM stage, still the real point hit by the laser (seem by FESEM) was different. This clearly revealed a shift between both images. Hence, the only means of correlating the electronic and the CCD images was to electronically shift the SE image.

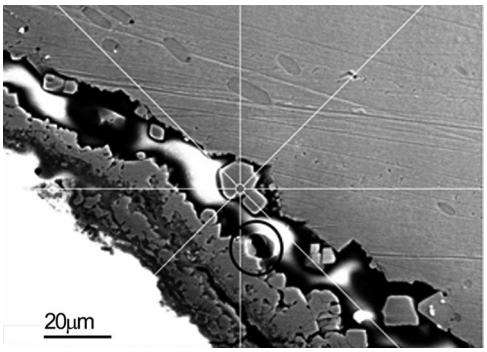

Fig. 1. SE image of a cross-section made of fresh and weathered Cu layers. Crosshair indicates the theoretical analysed spot in a Cu grain while the circle shows the real laser position impinging in the resin.

Thus matching accurately both beams is more troublesome and time consuming than reported elsewhere (Worobiec *et al.*, 2010) since it is less obvious than one would expect, even more in a FESEM were images are rotated 90°. This is partially due to the fact that although the laser hit is reproducible with micrometric precision, the electron beam is affected by different FESEM settings conditions. Indeed it is well known that the electron beam, the scanned area and hence the acquired electron images are affected by several fixed SEM factors such as electron acceleration voltage, electron beam current, aperture size, SEM vacuum conditions and working distance (WD), among others. Therefore SEM images drift whereas both the SCA optical images (from RS) and thus the laser beam position remain constant.

Consequently, we designed a strategy to correlate both illumination systems and assure exact alignment between the laser and electron beams, even when the ROI cannot be recognized by means of the SCA's video source. That is, we had to design a procedure to work in 'blind conditions' i.e. without the possibility to compare the SEM image with the reference image obtained with the SCA image. This is a time-consuming process which requires extensive experience and knowledge in SEMs background. In short, the designed strategy consists of referencing the electron image drift with respect to the fixed optical image using the FESEM stage coordinate system. Next, both images were correlated by shifting the electron beam to obtain the exact matching of both (electron and laser) beams. To do so, we innovated by using a Si wafer since it has very well defined and identifiable features, both under video signal of the SCA and with FESEM, at different resolution levels and scales. Moreover, it has a dimension similar to the laser spot size, *ca.* 1 μm (Figs. 2A,B).

As mentioned, there are SEM-related parameters which affect the electron beam shifting SEM images. During our work, we confirmed that a mismatch between both images occurred when changing whichever of these parameters; for instance,

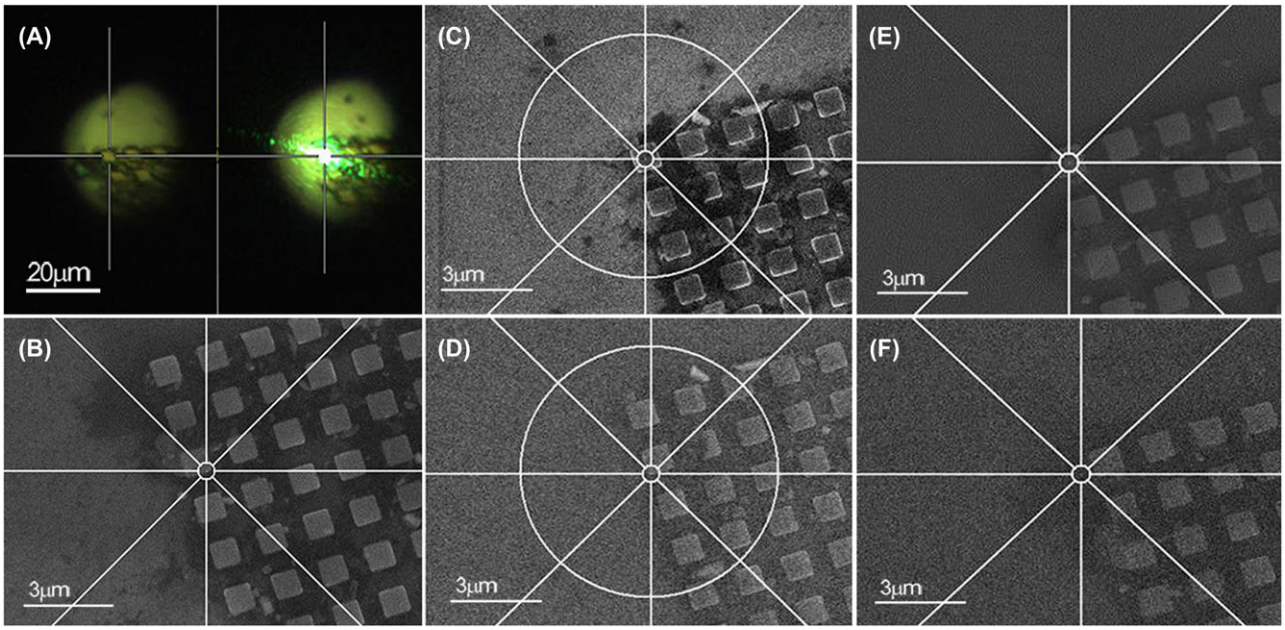

Fig. 2. (A) SCA optical image of Si wafer taken with the laser off (left) and with green laser (right), (B) corresponding FESEM image before shifting the electron beam to exactly match the electron and laser beams. FESEM images of Si wafer showing image drifting produced by: (i) changing the vacuum mode (C) HVC and (D) LVC; (ii) placing the SCA arm outside (E) and inside (F) the FESEM.

varying FESEM vacuum modes (Figs. 2C,D), aperture conditions or analysing samples with different conductivities. Moreover, the mere insertion of the SCA arm into the FESEM stage produces an electromagnetic disturbance in the electron beam path that results in electron image drift (Figs. 2E,F). Other factors to be considered include lens hysteresis, accumulation of charges, and thermal and mechanical drift of samples.

In our experience, relocation of a ROI when FESEM set-up conditions are changed is the most critical aspect to consider when working with a SEM–SCA system. This procedure is time-consuming but its neglect will result in analytical errors. In this regard, the parameter most often changed is the WD, whose optimal values for EDX acquisition and Raman analysis are different. In our VP-FESEM–SCA, the best WD to obtain EDX analyses is *ca.* 7–8 mm, whereas the required WD to insert the SCA probe into a FESEM stage is *ca.* 14 mm (these distances change depending on the SEM–SCA combination). Thus it is essential to move the stage from EDX WD to Raman WD. Figure 3 shows a flow chart to illustrate the proposed VP-FESEM–SCA optimized analytical procedure.

Raman signal intensity under different VP-FESEM vacuum environments

According to Worobiec *et al.* (2010) Raman intensities recorded under vacuum mode using SEM–SCA were up to 10 times lower than those acquired with MRS in ambient air. By contrast, Wille *et al.* (2014) recorded lower intensities by factors ranging between 30 (785 nm laser) and 150 (514.5 nm laser). However, the literature has not yet reported whether Raman signal intensities vary according to different vacuum modes selected within a VP-SEM. To examine this topic in depth, and prior to testing in our VP-FESEM–SCA Raman signal variations under HVC (10^{-6} Torr) and LVC (133 Pa) on a Si wafer (key Raman band at 520 cm^{-1}), we tested the loss of Raman signal intensity of the Si wafer with ambient air MRS. We intentionally chose the Si wafer since (i) as a standard it has physical and chemical stability which made it ideal for such a study, (ii) it is highly conductive and allows investigation at HVC and, (iii) any change recorded will be due to the vacuum. Raman set-up conditions were similar for both MRS and VP FESEM–SCA instruments. A 785 nm laser was used (saturation was achieved with the 532 nm laser) and 10 spectra were acquired with 10s exposure time. In agreement with Worobiec *et al.* (2010) and Wille *et al.* (2014) we found that Raman intensities in our VP-FESEM–SCA are *ca.* 90% lower compared to those obtained with MRS (Table 1). Certainly this is an important drawback of the SEM–SCA technique, particularly when compounds made of both organic and inorganic materials are analysed, such as paint layers made of pigments and binders. Indeed, during this study we confirmed how challenging it is to identify Raman bands for specific pigments due to the intense fluorescence caused by the organic binders. On the other hand binders remained unidentifiable in concordance with the results from Otieno-Alego (2009).

Next, to tackle Raman signal intensity under different FESEM vacuum modes we analysed, in addition to the Si wafer, a nonstandard sample, namely a *ca.* 2 mm calcite crystal (key

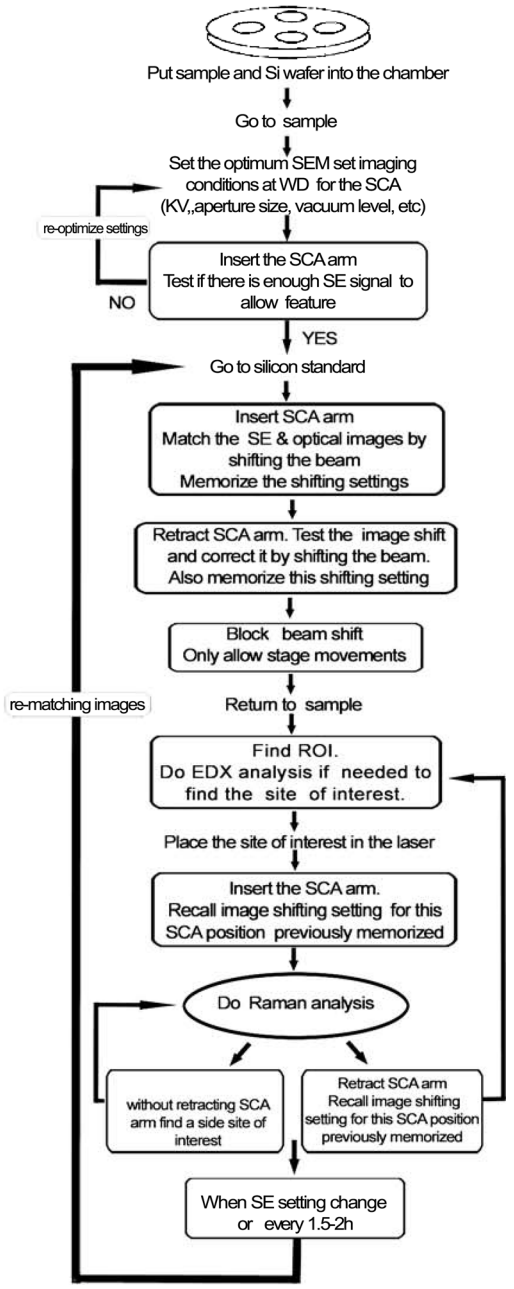

Fig. 3. An illustrative flow chart of the proposed VP-FESEM–SCA optimized analytical procedure.

Table 1. Raman signal intensities for Si wafer at 520 cm^{-1} performed with MRS (ambient air) and FESEM–SCA (HVC = 10^{-6} Torr). Analyses were done at different laser powers using a 785 nm laser

Laser power	MRS	FESEM-SCA
10%	49 367	5621
100%	39 5709	48 765

Table 2. Analyses of Si Raman band at 520 cm^{-1} with the FESEM–SCA system at different vacuum modes, lasers types and laser powers. § = standard deviation (%)

Laser		LVC (133 Pa)		HVC (10^{-6} Torr)	
type	Power (%)	nº counts	§	nº counts	§
785 nm	25	12.750	4	11.620	1
	35	16.500	1.8	15.570	0.8
	100	48.350	0.7	48.800	0.7
532 nm	13	5.020	6.7	5.370	2.1
	35	13.400	2.9	13.280	2
	100	40.500	1.7	40.000	2.1

Table 3. Analyses of calcite Raman band at 1086 cm^{-1} with the FESEM–SCA system at different vacuum modes and laser powers using the 532 nm laser. § = standard deviation (%)

Laser		LVC (133 Pa)		HVC (10^{-6} Torr)	
type	Power (%)	nº counts	§	nº counts	§
532	0.3	95	10	65	10
	8	1270	5	1370	5.8
	13	2330	3	2410	2.7
	35	6240	2.5	6500	3
	100	18 750	1.2	19 200	1.7

Raman band at 1086 cm^{-1}). Ten recorded spectra with 10 s exposure time were acquired from both samples using different laser types and powers. The Si wafer was analysed with both the 532 nm and the 785 nm laser (Table 2). Likewise calcite was analysed with both lasers though only results using the 532 nm laser are shown (Table 3) since those obtained with the 785 nm laser were rejected due to low Raman intensities. As Tables 2 and 3 show Raman intensities for each sample are similar under both FESEM vacuum modes irrespective of the type of laser used. Tables also show that standard deviations of Raman signals decrease when using higher laser powers under LVC and HVC. Moreover, for the Si wafer standard deviations of data acquired with both lasers are lower under HVC, whereas for calcite standard deviations at LVC and HVC are similar. Additionally, the variability of intensity in the Si key Raman band and the calcite key Raman band was determined through the acquired Raman series to obtain the average number of counts and the standard deviation. Thus we obtain for each intensity and vacuum mode the variability in the number of counts to confirm that the changes are meaningful. We found for both samples a slight difference in band intensities. For instance, in the Si wafer analysed with the 532 nm laser at 100% laser power, the difference accounted for 1.7% and 2.1% under LVC and HVC, respectively (Fig. 4). By contrast, for calcite (same analytical conditions) the difference accounted for 1.2% (LVC) and 1.7% (HVC).

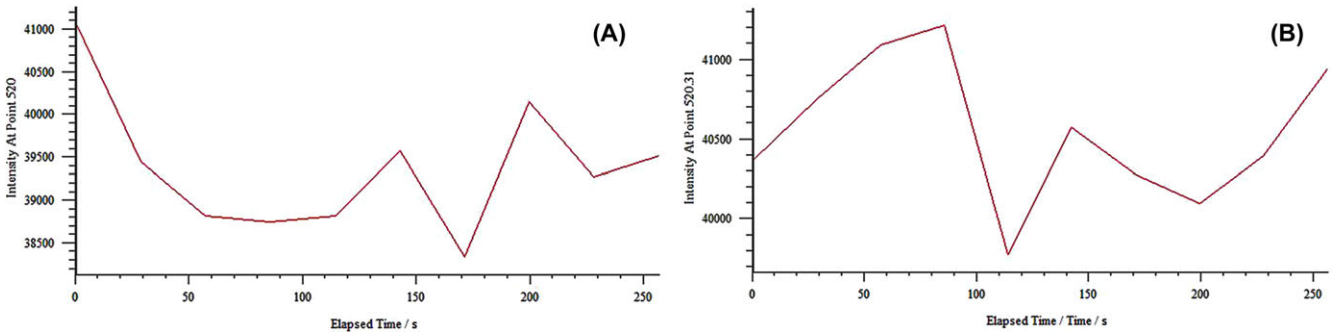

Fig. 4. Raman spectra comparison of Si wafer at 520 cm^{-1} acquired at HVC (A) and LVC (B) with the FESEM–SCA. Notice that difference in intensities is minimal.

All in all results demonstrate that Raman signal intensities are comparable working at different vacuum modes inside the VP-FESEM–SCA. Also in agreement with other authors (Worobiec *et al.*, 2010; Wille *et al.*, 2014) we found that Raman signal intensities in our FESEM–SCA were lower compared to the intensities acquired with MRS, though in different percentages to those reported elsewhere.

In this regard Worobiec *et al.* (2010) attribute the reduction in Raman intensities in the SCA to a signal loss during transmission through the optical fibre. This seems unlikely considering that signals travel along the fibre with minimal power loss due to very efficient total internal reflection of the laser inside the fibre. Furthermore, increasing the length of the fibre does not result in a significant decrease in delivered power. Instead Wille *et al.* (2014) ascribed Raman signal loss to the parabolic mirror present in the in-SEM Raman system as well as the Raman scattering efficiency of analysed minerals. Our experience is that other critical factors also affect Raman signal intensities. A crucial one is the launch of the laser into the optical fibre. The laser must be precisely aligned with the fibre to avoid signal loss. Moreover and consequentially, alignment should be verified by measuring the delivered laser power. Another key factor that can diminish Raman signals is the correct orientation of filters with respect to the optical fibre head. Incorrect filter setting can mean that nominal values of filters often are not genuine. Other factors that may lead to power transmission loss are unsuitable fibre core diameter and filter contamination.

Amorphous carbon deposition

Carbon deposition onto surface samples exposed to an electron beam is problematical for in-SEM Raman systems (particularly under LVC) since growing carbon layers compromise both SEM images and Raman signals. The severity of this problem depends of SEM accelerating voltage, probe current, sample exposure time under the electron beam, and SEM vacuum modes, among others factors. If any of these parameters increase, then the rate of carbon deposition increases, except for HVC (inverse relation). In this regard FESEMs are the best for preventing carbon deposition (specifically working at HVC) since they preserve excellent vacuum conditions. However, it is worth noting that one of the benefits of working with variable pressure SEM in the SCA is that nonconductive samples do not need to be carbon coated to avoid charging effects. Indeed this is a reason for the high demand for variable pressure SEM–SCA in artwork samples, and a *sine qua non* condition to acquire realistic Raman analyses, since carbon is Raman active and will mask other Raman signal from the ROI.

To address this issue, we studied a pigment that yield high quality Raman spectra, i.e. cinnabar (HgS) and for comparison purposes the polyester resin used to create the paint stratigraphy. Both are present in a multilayered historical paint sample prepared as a polished thin section described elsewhere (Fig. 5; Cardell *et al.*, 2009). Resin was examined because electrons raised from the SEM colliding in the organic layer will surely have collateral effects in the quality of Raman signals of pigments and binders (e.g. increasing fluorescence that complicates Raman band identification).

The intensity increments of the characteristic D and G graphite Raman bands (at 1385 and 1560 cm^{-1}, respectively) were checked in the cinnabar and resin once these materials had been exposed during 1 h in the FESEM stage (Figs. 6A,B). Analyses were done with a 532 nm laser at 0.3% laser power to minimize laser-induced damage. Six spectra with 1 s exposure time were acquired every 10 min. A carbon layer accumulated on the cinnabar and resin surfaces was expected after 1 h of laser exposure, mainly on the resin (due to its organic nature). Results revealed that in the resin the Raman background (termed fluorescence by Wille *et al.*, 2014) increased progressively over time (particularly at high wavelengths) although an increase in a specific graphite Raman band was not observed (Fig. 6C). Instead, an increment of the G graphite Raman band was recorded during Raman acquisition from cinnabar (Fig. 6D). Hence our results reveal that carbon deposition is substrate dependent. The growth of the carbon layer can compromise Raman signals to the point that their recognition becomes difficult. Thus during Raman

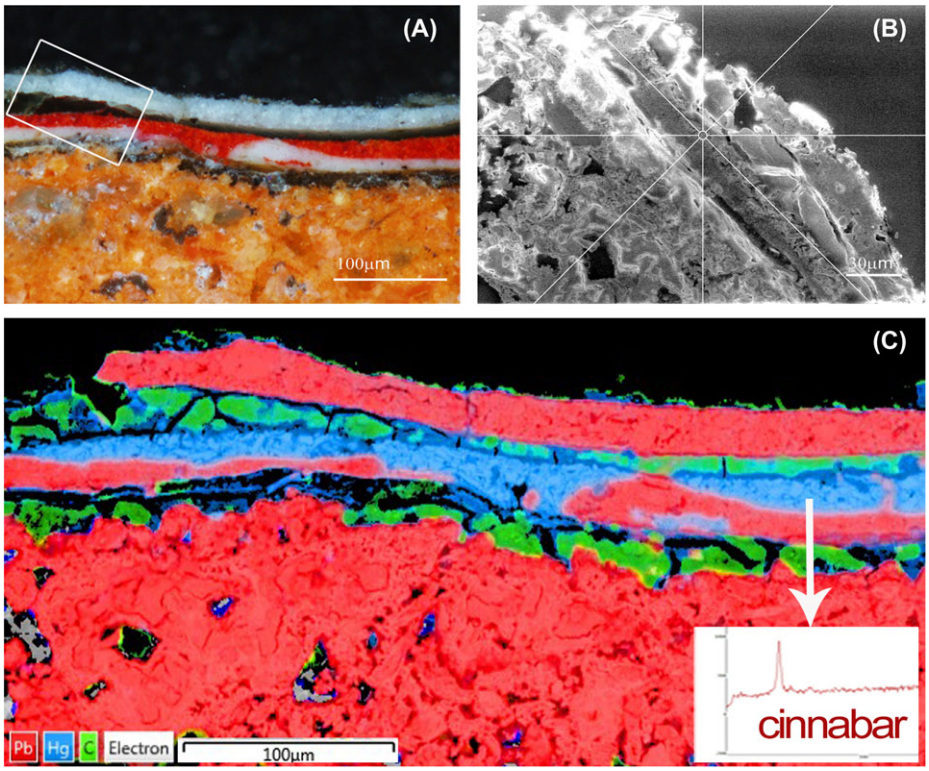

Fig. 5. (A) Photomicrograph showing the paint stratigraphy of a polychrome on wood from the Alhambra monument (Granada, Spain). From the inside out the layer sequence is: artificial minium, organic layer, cinnabar, organic layer and white lead layer at the surface. (B) FESEM photomicrograph showing the analysed cinnabar grain (crosshair). (C) A false-colour mineral map elaborated from SEM-EDX elemental mappings in the paint stratigraphy of (A).

spectra acquisition the electron beam must be turned off to reduce unnecessary beam bombardment, which can result in sample damage and/or excessive carbon deposition. On the other hand it is worth noting that carbon deposition also results from improper cleaning of the SEM stage; to avoid this, plasma cleaners are highly recommended.

Crystal nature and size

During our investigations, apart from sample damage caused by the FESEM electron beam (not explained here), it became clear that laser-induced damage (mineral transformation) and decrease of Raman signal intensity took place on some pigments. Factors initiating damage processes such as oxidation/reduction and phase transformation causing molecular, elemental or physical changes include the atmosphere (vacuum/air modes), laser beam intensity, sample preparation or particle structure. Laser-induced damage on pigments analysed with RMS has been widely reported (Burgio & Clark, 2001; Navas *et al.*, 2010) as has damage to particles (aerosols) studied with SEM–SCA (Stefaniak *et al.*, 2006, 2014; Worobiec *et al.*, 2010, 2011). Worobiec *et al.* (2010) state that particle damage due to the laser beam is more troublesome when applying SEM–SCA than the stand-alone MRS. These authors suggest means of decreasing or eliminating damage when applying both techniques. They propose that particles should be prepared as thin sections to be studied with SEM–SCA. However, as we will discuss next, during our analyses we verified that intense laser-induced heating occurs in minerals which are part of cross-sections prepared as polished thin sections. This is a critical issue that deserves more investigation since often samples from cultural heritage are prepared as thin sections.

To shed light on the effect of pigment nature and size in the decrease of Raman signals and mineral transformation we studied pigments mixed with binders embedded in paint layers, and loose pigments of different size. To address laser-induced damage depending on pigment nature, we studied cerussite ($PbCO_3$) and cinnabar (HgS) pigments present in diverse layers of the paint stratigraphy shown in Figure 5. Pigment selection was guided by their differing responses to laser irradiation in the FESEM–SCA system. Although cerussite was a very heat-sensitive mineral to Raman analyses performed with our hybrid system, yielding slight Raman signals, cinnabar produced high-quality Raman spectra, and no phase transformation into metacinnabar was recorded with increasing laser exposure time. Thus we did time-lapse analyses to address laser-induced damage in cerussite. Raman analyses

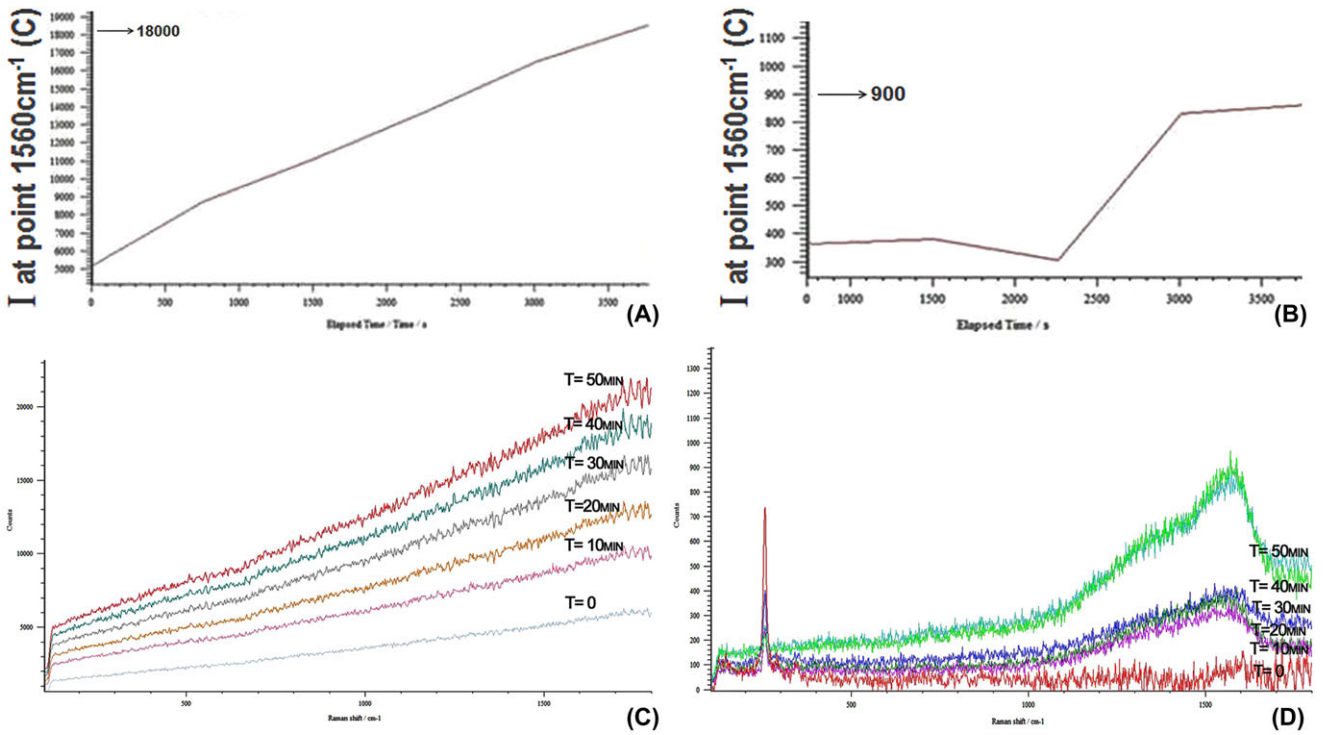

Fig. 6. FESEM–SCA analyses on cinnabar and resin layers showed in Figure 5. Intensity increase in G graphite Raman band at 1560 cm^{-1} measured on resin (A) and on cinnabar (B). Resin baseline increment during Raman acquisition times (C). Increase in G graphite Raman band measured on cinnabar during Raman acquisition (D).

were acquired using the lowest laser power that produces a Raman signal and then power was slowly increased checking the laser power that cerussite could tolerate prior to damage. As a result, we realized (as expected) that it is crucial to have a wide range of attenuation filters to diminish the incident laser beam. Initially we had 10%, 25%, 50% and 100% transmitting filters.

During our work, we confirmed that the actual transmission (real values) of some filters were different from their nominal (theoretical) values, making it even more difficult to control in-FESEM Raman analyses. Our experience is that historical paints made of closely mixed pigments and binders are very sensitive to high laser beam intensities. Thus it is critical to have more attenuation filter options below 10% (Otieno-Alego, 2009) since laser powers higher than this value are barely used to analyse historical paints due to collateral damage effects. Accordingly, we incorporated transmitting filters of 0.5%, 1%, 2.5%, 5% and 8%, as well as the possibility to obtain infinite low laser intensities by tuning laser beam intensities using an electronic device. However, when laser power is too low the Raman bands either can disappear into the noise or not be identified correctly.

Considering the above, we analysed cerussite (key Raman band at 1053 cm^{-1}) with the FESEM–SCA using the 532 nm laser at increasing laser powers up to 8% since this laser power does not damage cerussite at the first Raman acquisition and produces enough signal to register heat damage from the second acquisition. A sequence of 10 recorded spectra with 10 s exposure time and 10 s time lapse were acquired. Results revealed that during Raman signal acquisition (255 s) the 1053 cm^{-1} Raman band was decreasing. Concurrently Raman signal at 142 cm^{-1} of massicot (PbO yellow rhombic) was appearing (Fig. 7) which indicates that the laser was damaging the cerussite surface. The maximum band intensity for massicot was attained at *ca.* 142 s after the start of the analyses. This result shows that it is crucial to examine Raman signals from the first acquisition moment to check if mineral modifications are occurring. Otherwise false interpretations and conclusions can be inferred.

Laser-induced damage was checked by analysing a cinnabar (key bands at 252 and 343 cm^{-1}) crystal during 1 h using the 532 nm laser at its lowest power of 0.3%. Six recorded spectra with 10 s exposure time were acquired every 10 min. As shown in Figure 6D the Raman band at 252 cm^{-1} decreased during signal acquisition and disappeared nearly completely after 40 min. Unexpectedly, Raman bands of others minerals were not found, while concurrently a strong increase of the D and G bands of graphite appear. To clarify this, we found it crucial to record the cinnabar Raman spectrum over the wavenumber range between 100 and 3500 cm^{-1}. Thus we could observe the parallel increase of the G graphite band at *ca.* 1560 cm^{-1}. Our hypothesis is that the growing thickness of the

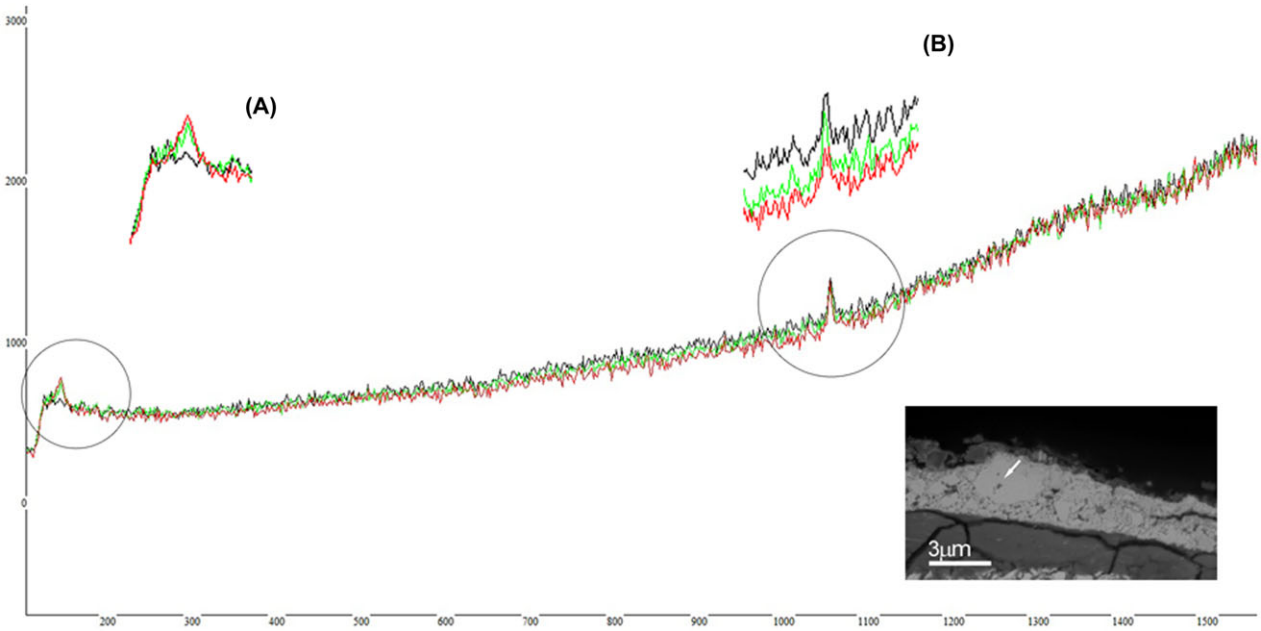

Fig. 7. FESEM–SCA study of cerussite transformation (1053 cm^{-1}) towards massicot (142 cm^{-1}). Spectrum is scaled at band of maximum intensity (1056 cm^{-1}). Notice the decreasing bands of cerussite (inset B, spectrum not scaled) and the growing up of massicot bands (inset A). Acquisition times are: blue = 10 s; green = 142 s and red = 255 s.

carbon layer somehow hinders cinnabar from emitting Raman signals.

Our finding agrees with those of Béarat *et al.* (2008) which showed laser-induced alteration in cinnabar crystals (colour change) and loss of Raman intensity in its characteristic bands; likewise no phase transformation into a new phase (i.e. metacinnabar) was recorded. These authors attribute this phenomenon to cinnabar chemical change (specifically, loss of sulphur) and physical change via reconfiguration and expansion of its crystal lattice.

The relationship between Raman signal intensity and crystal size was tackled analysing stand-alone calcite (key Raman band at 1086 cm^{-1}) pigments with different sizes ($\varnothing \leq 10$–100 μm). A 532 nm laser was used at 8% laser power to acquire 1 spectrum at 10 s exposure time in the VP-FESEM–SCA. We started analysing a 100 μm calcite crystal and continued with crystals of fewer dimensions ending with one of *ca.* 10 μm in size. As Figure 8 shows the Raman spectrum of the 100 μm calcite crystal yields a decent band at 1086 cm^{-1} whereas diminished for crystals of 20 and 15 μm in size. Finally this key Raman band does not appear analysing the 10 μm calcite crystal. Therefore, the critical size for calcite crystals analysed with our FESEM–SCA to produce identifiable Raman bands is *ca.* 10 μm. Apart from crystal size it must be considered that Raman recognition of a substance is strictly dependent upon its intrinsic nature. Indeed Pointurier & Marie (2013) reported that U-rich particles as small as 1 μm were analysed via a SEM–SCA system, whereas Stefaniak *et al.* (2014) were able to analyse uranyl fluoride particles of *ca.* 700 nm when deposited on exceptionally smooth substrates.

Additionally, we performed a similar study with MRS in calcite crystals of different sizes to check the trend found with FESEM–SCA. Rationally due to the small size of crystals analysed with FESEM–SCA, the MRS study was conducted in different samples. In this case the test was done in so-called fine calcite powder with particles sizes below 200 μm, and coarse calcite powder with particle size above 800 μm (Kremer Pigments GmbH & Co. KG, Vigo, Spain. Pigment reference K11416, φ = 120 μm and 1 mm. Particle sorting achieved via sieving). Results revealed that Raman signal intensity decreased in the calcite fine powder *ca.* 35% compared with the signal intensity acquired in the coarse powder (Fig. 9).

Depth of focus

During our work analysing target features with the FESEM–SCA we noticed variations in the intensity of Raman signals even with the same laser settings analysing the same ROI. We supposed that these dissimilarities were related to the focusing process to perform Raman analyses on such areas. One of the greatest benefits of SEM images is their great depth of focus, which allows examination of surfaces much rougher and at much higher magnifications than using a light microscope. Thus identification of an ROI is more accurate and faster using SEMs than with MRS. Consequently, the difficulty working with SEM–SCA is that while the SEM image is focused, the white light image seen with the Raman system may not be.

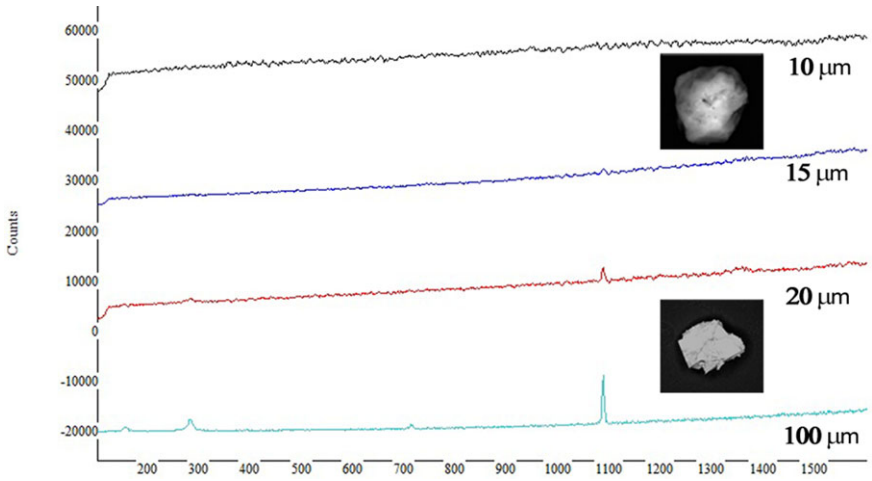

Fig. 8. Raman spectra of calcite crystals with different sizes acquired with the FESEM–SCA. Note that Raman signals diminished and finally disappeared with decreasing crystal dimension.

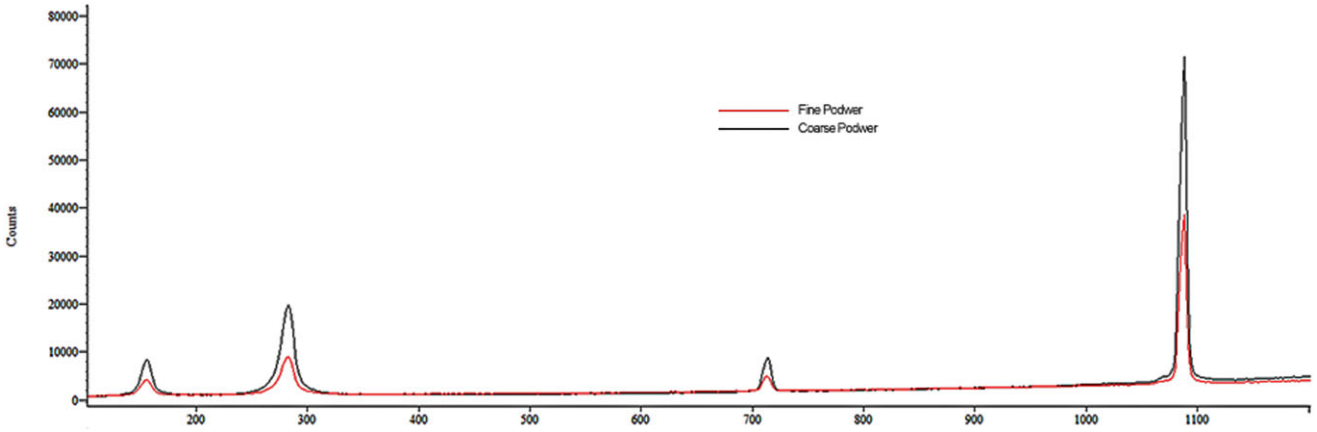

Fig. 9. Raman spectra of calcite (A) fine powder and (B) coarse powder acquired with MRS. Note the Raman signal intensity decrease in the fine powder.

To shed light on this topic we did in-, over- and underfocused Raman analyses on calcite crystals with sizes of *ca.* 100 μm. Note that the Raman ROI is defocused in situations of under and over focus, but in all cases the corresponding SEM images are focused. In-FESEM Raman analyses were done with the 532 nm laser at 100% power intensity and 10 accumulations of 1 s exposure time. Results revealed that number of counts registered for in-focus conditions was 22.200 ± 600, whereas the highest Raman band intensity was acquired with overfocus (29.400 ± 500 counts) and the lowest one was recorded with underfocus (15.700 ± 300 counts; Fig. 10). The inferences raised from this study are 2-fold: (i) small variations in WD working with SEMs do not imply changes of focus in SEM images. However, minor differences strongly affect Raman intensities since they produce large changes in the focus of the laser beam; and (ii) in our hybrid system the Raman signal intensity increases with slight over focus. This issue should be checked for other SEM–SCA combinations in order to generalize this statement.

Surface-enhanced Raman scattering (SERS)

Raman signals are inherently weak. SERS is a method to amplify weak Raman signals to overcome the traditional drawback of Raman scattering. In brief, the enhancement takes place at a metal surface which has nanoscale roughness or due to deposition of metallic nanoparticles in films (colloidal solutions) on the analyte. Many researchers create their own SERS substrates, but there are also commercially available platforms (Fan *et al.*, 2011). SERS is receiving much attention in the field of cultural heritage, since it increases confidence in identification of historic pigments (Whitney *et al.*, 2006; Frano *et al.*, 2014). SERS has also been used for bacterial (Jarvis *et al.*, 2004) and environmental particle identification (Worobiec *et al.*, 2010) using in-SEM Raman systems.

To examine this topic we studied the SERS effect in paint samples grouped in two categories: (i) loose calcite pigments and (ii) complex cross-sections prepared as polished thin sections. We started analysing samples with the simplest

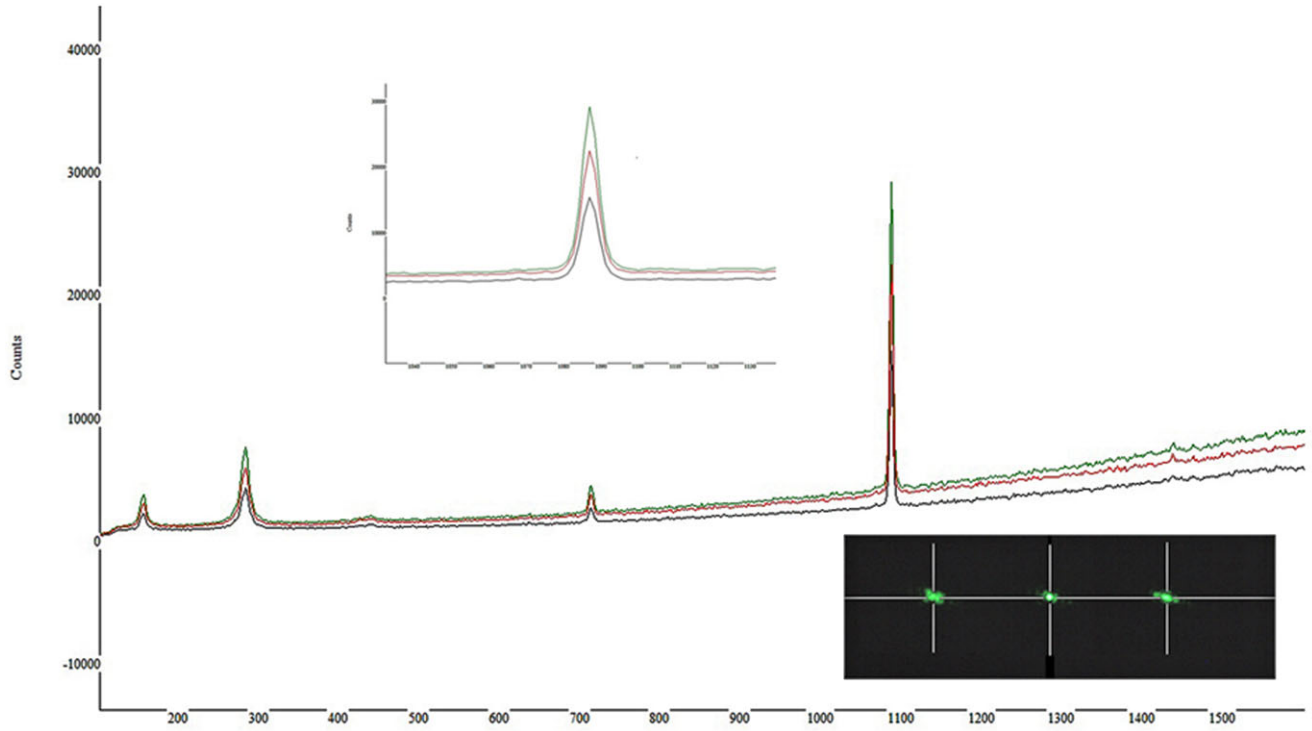

Fig. 10. Raman spectra of calcite acquired under (black), over (green) and in-focus (red). Spectrum is normalized to the highest band (1086 cm^{-1}), thus inset shows variation in Raman intensities at such band. Inset figure shows that Raman ROI is defocused in situations of under (left) and over focus (right).

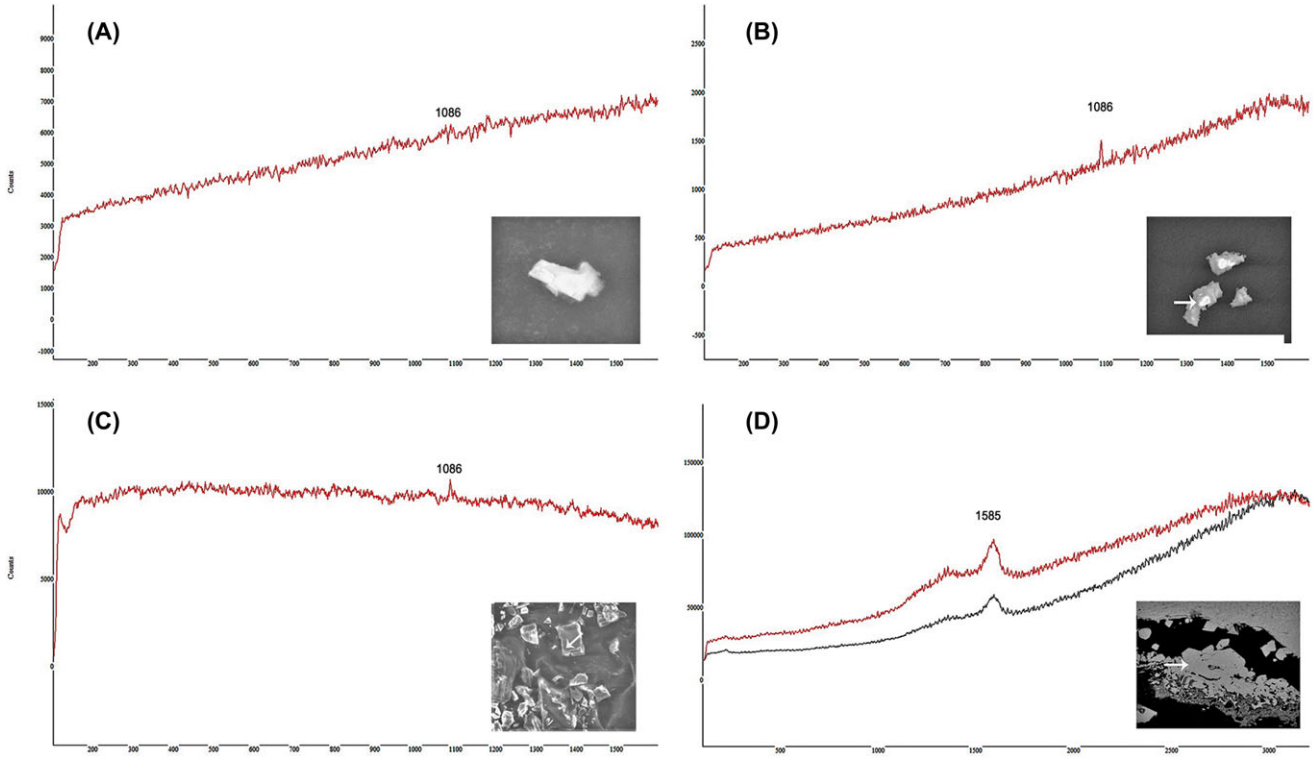

Fig. 11. Raman spectra for 10 μm calcite crystals mounted on C tapes not sputtered with gold (A), sputtered with gold (B), mounted on Al tape (C) and for a Cu-rich archaeological sample prepared as thin section before (black) and after (red) sputtering with gold (D).

composition and structure. Raman analyses were done using the 532 nm laser at 8%. Three recorded spectra were acquired from each ROI with a 10s exposure time. SERS was checked in stand-alone calcite crystals with size *ca.* 10 μm since no active calcite Raman bands were recorded (see Fig. 8). These crystals were mounted onto pin stubs using either Al or C double-sided tape. In this way the Al substrate exhibiting a roughened surface worked as a SERS platform itself. Other crystals were mounted onto C tapes and sputtered with gold. Care was taken to perform a slight sputtering to obtain a noncontinuous film (i.e. isolated gold particles up to 3 nm), as no SERS effect was achieved with uniformly thick gold films. Figure 11(A) shows that no calcite band at 1086 cm^{-1} was seen analysing the crystal placed on the C tape and without gold coating. Instead this band is seen discernible for the calcite mounted on the C tape covered with gold (Fig. 11B) and for that mounted on the rough Al tape (Fig. 11C).

Working with thin sections, we started analysing the archaeological sample made of Cu layers (see Fig. 1) without organic binders that produce fluorescence interfering Raman signals. Figure 11(D) shows the spectra before (black) and after (red) sputtering this thin section with gold. Although no clear Raman bands could be attributed to Cu-bearing compounds, it is clear that the SERS effect causes an increase on both the baseline and the Raman bands attributed to graphite (~1400 and 1585 cm^{-1}).

In the multilayered paint cross-section (Fig. 5) we checked the SERS on cerussite crystals (that yields slight Raman signals) and on cinnabar crystals (that produce intense Raman bands) using both the 532 nm and the 785 nm laser. In neither of the pigments was an enhancement of Raman bands clearly observed, which we attribute to the fact that both are closely mixed with organic binders and form part of a complex, structured sample embedded in resin. To shed light on this topic other sample preparation strategies for SERS effect are under study.

Concluding remarks

The novel SCA technique shows great potential to characterize complex compounds at micro- and nanoscales in diverse fields such as life science, geoscience and heritage science. However, analysing closely mixed inorganic and organic components present in the same sample, such as pigments and binders in paint stratigraphies, is a critical aspect not yet resolved. As stated elsewhere, Raman bands associated with organic binders in the presence of inorganic matter cannot be assigned with certainty. We found that the opposite is also true; acquiring a decent Raman signal from an inorganic pigment mixed with organic binders is fairly challenging. Ongoing investigations are tackling the influence of various sample preparation methods, including different sample substrates and resins (used to embed the paint stratigraphies) to better discern Raman fingerprints from pigments and binders, since so far binders could not be identified.

The most relevant conclusions and recommendations of this work are:

(i) The key aspect to tackle working with FESEM-EDX–SCA is relocation of a ROI. The first step should be to define and fix the best specific FESEM operating conditions to analyse a ROI prior to performing Raman analyses. Clearly once the correlation between the electron and the optical images are established, none of the FESEM operating parameters must be changed, otherwise the electron image will drift. Moreover, for each FESEM operating condition and type of studied ROI, correlation between the laser spot and the SEM image needs to be regularly tested and corrected. Accordingly, the laser position on the SEM image needs to be checked regularly. The frequency of testing mainly depends on the micrometric precision required for the analyses. Matching both images is time consuming and relies on operator expertise. The above cited problems have to be resolved specifically for each particular SEM–SCA combination, since each SEM brand and model have their own technical specifications (conventional, high resolution, SEM stage geometry, EDX detector geometry, etc.). The solutions have to be established for each combination with the aid of their specific software and/or resources.

(ii) We recommend that for each SEM–SCA configuration the loss of Raman signal intensity should be determined.

(iii) The degree of carbon deposition on a sample depends on the nature of the analysed component. We suggest acquiring Raman spectra at regions over 1600 cm^{-1} to detect graphite Raman bands that could provide clues to accurately interpret difficult Raman spectra.

(iv) We suggest that thickness of gold sputtering must be controlled since over-sputtering might hinder Raman signals.

(v) Raman signal quality depends on mineral size and nature. Crystals with more volume provide better Raman spectra and are less affected by laser damage. Since the analytical procedure is based on trial and error, one should proceed with caution using the lowest laser power possible and later increasing doses. Damage depends not only on laser wavelength excitation, laser power and laser exposure time, but also strongly on the nature and size of the analysed minerals. Two factors are involved: (i) in SEM–SCA systems heat cannot be evacuated from sample due to absence of atmosphere, and, (ii) studied features are much smaller in SEM–SCA than in MRS. Thus, samples are more likely to burn since they are more susceptible to heat damage and so unravelling their nature is more difficult.

(vi) We recommend to cautiously planning the analysis strategy for each study target. Although at first this can be time consuming, in the end it will guarantee reliable results.

Acknowledgements

Financial support was provided by the Andalusian Research Group RNM-179 and Spanish Research Projects AERIMPACT (CGL2012-30729) and EXPOAIR (P12-FQM-1889). The authors thank A. Yebra for MRS analyses, A. Kowalski for English revision and two anonymous referees whose comments improved the paper. FESEM–SCA analyses were performed at the Scientific Instrumentation Centre (CIC) of the University of Granada (Spain).

References

Béarat, H., Chizmeshya, A., Sharma, R., Barbet, A. & Fuchs, M. (2008) Mechanistic and computational study of cinnabar phase transformation: Applications and implications to the preservation of this pigment in historical painting (ed. by T.S. Akasheh), pp. 53–70. Foundacion El Legado Andalusi, Spain.

Bersani, D., Lottici, P.P., Virgenti, S., *et al.* (2010) Multi-technique investigation of archaeological pottery from Parma (Italy). *J. Raman Spectrosc.* **41**, 1556–1561.

Brooker, A.D., Baldwin, J.W., Pehrssohn, P.E. & Butler, J.E. (2003) Structural and Chemical Analyser for SEM studies of nanostructures. *Microsc. Microanal.* **9**, 1110–1111.

Brooker, A.D., Jarvis, R.M., Goodacre, R., Bennett, R., Dawe, C.J., Leak, D.J., Lainchbury, M.J. & Hill, M.R. (2004) A structural and chemical analyser (SCA) identification of bacteria labelled by metallic nanoparticles. *Microsc. Microanal.* **10**, 932–933.

Burgio, L. & Clark, R.J.H. (2001) Firth, S. Raman spectroscopy as a means for the identification of plattnerite (PbO_2), of lead pigments and of their degradation products. *Analyst* **126**, 222–227.

Cardell, C., Guerra, I., Yebra-Rodríguez, A. & Van Grieken, R. (2013) Addressing problems raised from analysing mineral samples by coupled Raman Spectroscopy–High Resolution Variable Pressure SEM/EDX, pp. 75. Technart 2013, PP16, Amsterdam, the Netherland.

Cardell, C., Rodríguez-Simón, L., Guerra, I. & Sánchez-Navas, A. (2009) Analysis of Nasrid polychrome carpentry at the hall of the *Mexuar* palace, Alhambra complex (Granada, Spain) combining microscopic, chromatographic and spectroscopic methods. *Archaeometry* **51**, 637–657.

Fan, M., Andrade, G.F.S. & Brolo, A. G. (2011) A review on the fabrication of substrates for surface enhanced Raman spectroscopy and their applications in analytical chemistry. *Anal. Chim. Acta.* **693**, 7–25.

Frano, K.A., Mayhew, H.E., Svoboda, S.A. & Wustholz, K.L. (2014) Combined SERS and Raman analysis for the identification of red pigments in cross-sections from historic oil paintings. *Analyst* **139**, 6450–6455.

Goienaga N., Sarmiento, A., Olivares, M., Carrero, J.A., Fernández, L.A. & Madariaga J.M. (2013) Emerging application of a structural and chemical analyzer for the complete characterization of metal-rich particulate matter. *Anal. Chem.* **85**, 7173–7181.

Gómez-Nubla, L., Aramendia, J., Fdez-Ortiz de Vallejuelo, S., Castro, K. & Madariaga, J.M. (2013) From Portable to SCA Raman devices to characterize harmful compounds contained in used black slag produced in Electric Arc Furnace of steel industry, *J Raman Spectrosc.* **44**, 1163–1171.

Hazekamp, J., Reed, M.G., Howard, C.V., Van Apeldoorn, A.A. & Otto C. (2011) The feasibility of Cryo In-SEM Raman microspectroscopy. *J. Micros.* **244**, 122–128.

Irazola, M., Olivares, M., Castro, K., Maguregui, M., Martínez-Arkarazo, I. & Madariaga, J.M (2012) In situ Raman spectroscopy analysis combined with Raman and SEM-EDS imaging to assess the conservation state of 16th century wall paintings. *J. Raman Spectrosc.* **43**, 1676–1684.

Jarvis, R.M., Brooker, A.D. & Goodacre, R. (2004) Surface-enhanced Raman spectroscopy for bacterial discrimination utilizing a scanning electron microscope with a Raman spectroscopy interface. *Anal. Chem.* **76**, 5198–5202.

Kawauchi, K., Ogura, K., Nielsen, C., Brooker, A.D. & Bennett R. (2004) Material analysis using SEM/EDS combined with a Raman spectrometer. *Microsc. Microanal.* **10**, 958–959.

López-Sánchez, P., Schumm, S., Pudney, P. & Hazekamp, J. (2011) Carotene location in processed food samples measured by Cryo In-SEM Raman. *Analyst*. **136**, 3694–3697.

Mireia, I., Olivares, M., Castro, K., Maguregui, M., Martínez-Arkarazo, I. & Madariaga, J.M. (2012) In situ Raman spectroscopy analysis combined with Raman and SEM-EDS imaging to assess the conservation state of 16th century wall paintings. *J. Raman Spectrosc.* **43**, 1676–1684

Navas, N., Romero-Pastor, J., Manzano, E. & Cardell, C. (2010) Raman spectroscopic discrimination of pigments and tempera paint model samples by principal component analysis on first-derivative spectra. *J. Raman Spectrosc.* **41**, 1486–1493.

Ospitali, F., Chiavari, C., Martini, C., Bernardi, E., Passarini, F. & Robbiola, L. (2012) The characterization of Sn-based corrosion products in ancient bronzes: a Raman approach. *J. Raman Spectrosc.* **43**, 1596–1603.

Ospitali, F., Bersani, D., Di Lonardo, G.F. & Lottici P.P. (2008) 'Green earths': vibrational and elemental characterization of glauconites, celadonites and historical pigments. *J. Raman Spectrosc.* **39**, 1066–1073.

Otieno-Alego, V.J. (2009) Some forensic applications of a combined micro-Raman and scanning electron microscopy system. *Raman Spectrosc.* **40**, 948–953.

Pointurier, F. & Marie, O. (2013) Use of micro-Raman spectrometry coupled with scanning electron microscopy to determine the chemical form of uranium compounds in micrometer-size particles. *J. Raman Spectrosc.* **44**, 1753–1759.

Prusnick, T., Brooker, A.D. & Bennett, R. (2004) The structural and Chemical Analyzer (SCA): a new analytical technique for SEM. *Microsc. Microanal.* **10**, 930–931.

Stefaniak, E., Worobiec, A., Potgieter-Vermaak, S., Alsecz, A., Török, S. & Van Grieken, R.(2006) Molecular and elemental characterisation of mineral particles by means of parallel micro-Raman spectrometry and scanning electron microscopy/energy dispersive x-ray analysis. *Spectroch. Acta Part. B* **61**, 824–830.

Stefaniak, E.A., Pointurier, F., Marie, O., Truyens, J. & Aregbe, Y. (2014) In-SEM Raman microspectroscopy coupled with EDX—a case study of uranium reference particles. *Analyst*. **139**, 668–675.

Toepfer, P. & Shearer, G.L. (2006) Combining SEM/EDS and Raman microscopy for the identification of contaminant particles in pharmaceutical products. *Microsc. Microanal.* **12**, 1646–1647.

Truchet, M. & Delhaye, M. (1988) Couplage d'une sonde Raman laser et d'une sonde de Castaingdans un microscope electronique (Molecular laser-Raman analysis and elemental electron-probe X-ray-analysis in transmission electron-microscope). *J. Microsc. Spectrosc. Electron.* **13**, 167–175.

Van Apeldoorn, A.A., Aksenov, Y, Stigter, M., *et al.* (2005) Parallel high-resolution confocal Raman SEM analysis of inorganic and organic bone matrix constituents. *J. R. Soc. Interface.* **2**, 39–45.

Whitney, A.V., Van Duyne, R.P. & Casadio, F. (2006) An innovative surface-enhanced Raman spectroscopy (SERS) method for the identification of six historical red lakes and dyestuffs. *J. Raman Spectrosc.* **37**, 993–1002.

Wille, G., Bourrat, X., Maubec, N. & Lahfid, A. (2014) Raman-in-SEM, a multimodal and multiscale analytical tool: performance for materials and expertise. *Micron.* **67**, 50–64.

Williams, K., Bennett, R., Brooker, A.D., Bormett, R. & Prusnick T. (2003) Methods in Raman spectroscopy—combining other microscopes. *Microsc. Microanal.* **9**, 1094–1095.

Worobiec, A., Darchuk, L., Brooker, A.D., Potgieterc, H. & Van Grieken, R. (2011) Damage and molecular changes under a laser beam in SEM-EDX/MRS interface: a case study on iron-rich particles. *J. Raman Spectrosc.* **42**, 808–814.

Worobiec, A., Potgieter-Vermaak, S., Brooker, A.D., Darchuk, L., Stefaniak, E. & Van Grieken, R. (2010) Interfaced SEM/EDX and micro-Raman Spectrometry for characterisation of heterogeneous environmental particles—fundamental and practical challenges. *Microchem. J.* **94**, 65–72.